

Smart Emergency Charging of Electric Vehicle with Solar PV-based Backstepping Model-Free and critic RL Control Structure

Karthikeyan K*, Anitha P**, Karthik Kumar K***, Kamaraja A S****

* *Department of Electrical and Electronics Engineering, Ramco Institute of Technology, Rajapalayam Tamilnadu, India*

** *Department of Electrical and Electronics Engineering, University VOC college of Engineering, Tuticorin, Tamil Nadu, India*

*** *Department of Electrical and Electronics Engineering, National Engineering College Kovilpatti Tamilnadu, India*

**** *Larsen and Toubro Technology Services, Chennai, Tamilnadu, India; (Email: kamaraja.as@gmail.com)*

Abstract: Customers are now also worrying about restricting factors in the Electric Vehicle industry like battery life, charge station location, power grid capacity, restricted drive range, and slow battery charging. However, there is a rise in Electric vehicles and Emergency Solar-to-Electric Vehicle Battery Charger (SEBC) is recommended. It offers a practical way to charge Electric cars in critical situations. Based on the state of charge (SOC), capacities, and vital factors, the proposed smart charger can charge another Electric vehicle. Smart chargers can control Output voltages and immediately deliver current into an Electric vehicle. These qualities are achieved by the model-free non-linear integral. The Back-stepping controller (MF-NIBC) is used for managing battery charger Output voltage. By using the critic networks with the deep deterministic policy gradient (DDPG), the MF-NIBC controller is adjusted. Though many solutions to these limitations have been put forth, it offers low efficiency and minimum cost-effectiveness. Therefore, this study proposes a brand-new battery charger called the Emergency Solar-to-Electric Vehicle Battery Charger (SEBC). Last but not least, real-time experiments based on the OPAL-RT configuration to verify the viability and application of the suggested Solar-to-Electric vehicle battery charging features.

Keywords: Electric vehicle, Quick charger, Sliding mode controller, System learning, Dual Active Bridge.

1. INTRODUCTION

The transport industry is rapidly switching from gas-powered cars to electric vehicles due to the pollution produced by these vehicles and their influence on climate change (Iyer et al., 2018). The Electric vehicle encourages low Energy use and minimizes carbon emission (Fuinhas et al., 2021; Gryparis et al., 2020). Yet, it includes the station's life span, speed of the charger, and access to the station for charging and the Electric vehicle industry usage is constrained by costs and travel lengths (Asna et al., 2021; Tu et al., 2019). The restricted range of EVs is the most important obstacle to their broad adoption (Krishna, 2021). People are concerned about their Electric Vehicle's battery running out while on long trips in places with no charging options.

To handle this, charging spots have been installed in both city and country areas. Yet, it is not enough to serve all EVs and these charging points are scant and somewhat apart in rural regions. Additionally, it is not cost-efficient (Sheng et al., 2021). Using this technique, EVs can assist one another by sharing 5–15 percent of the charge in their batteries in a critical situation. But, battery-specific details like charge condition, Voltages, current, capacities, and charging time are essential to assuring a secure and convenient system. Notably, the charger and charging procedure should have been made more reliable. By using smart controller, it can be accomplished.

Some control strategies include Model prediction controller (MPC) (Li et al., 2019), slide mode controller (SMC) (Ahmed et al., 2021; Mallik et al., 2018), Active Disruption Rejections Controller (ADRC) (Aboudrar et al., 2020), Backstepping controller (Song et al., 2021), and Long Short-Term Memory (LSTM) neural networks (Chang et al., 2021), have been devised by modern researchers for use with EV chargers. However, the majority of powerful controllers necessitate an in-depth recognition of the system model. These techniques are incapable of correctly stabilizing the Electric Vehicle charger when variability and unmodeled dynamics occur. To address this issue, Model-free Backstepping control can be used on systems without defining the model (Younes et al., 2016). Also, it includes certain parameters and it is developed using a variety of techniques, such as fuzzy logic, Meta heuristic algorithm, and neural network Zeitouni et al., 2020; (Gheisarnjad & Khooban, 2019) Wu et al., 2021). In (Precup et al., 2022), the iterative Feedback Tuning, Intelligent PID Controllers, Model-Free Sliding Mode Controllers, Model-Free Adaptive Controllers, Hybrid Model-Free and Model-Free Adaptive Virtual Reference Feedback Tuning controllers and Hybrid model-free and model-free adaptive fuzzy controllers were used for tuning process which was observed and studied. This procedure deals with the structural, operational, and behavioral components of the company, perceived as an intricate dynamic system, suggesting a design and administration technique modeled after the human brain,

in which the problem solving is accomplished through Perception — Memory — Learning and Action formation mechanisms (Dumitrache et al., 2021). The classical PI control technique based on Gradient Descent (GD) and the RL-based control approach utilizing the metaheuristic Particle Swarm Optimization (PSO) algorithm are compared. Experiments are conducted on a nonlinear servo system laboratory setup. Each technique is evaluated on its ability to solve the optimal reference tracking control problem for a laboratory position control system (Zamfirache et al., 2022). A novel testing methodology has been presented which is appropriate for multi rotor drones, featuring adjustable control parameters and real-time tracking of sensor data via wireless communication. It has the benefit of unrestricted motion along all axes without elevation motion, compared to already existing testing systems (Ucgun et al., 2022).

According to literature, the previous study showed clearly that the controller used for stability analysis and electric vehicle applications was not suitable for tuning. The main challenge posed by the combination of model-free and critic RL control is that each has its own set of strengths and weaknesses. Model-free RL is adept at adapting rapidly to changes in the environment and can learn from experience without much prior knowledge. Nevertheless, it is prone to weak generalisation performance and can take a long time to achieve convergence. Critic RL on the other hand learns faster, but demands a model of the environment to make predictions and updates. To incorporate these two approaches effectively, it is necessary to acquire sufficient data to create an accurate model of the environment, adjust the learning parameters to achieve a balance between the two approaches, and make sure that the model-free and critic RL do not compete but rather collaborate. The previous systems lagged behind in terms of voltage and current adjustment in the charging system. Therefore, the proposed system overcomes the above issues with the following motivations.

This study suggests and motivates an emergency Solar to Electric Vehicle Battery Charger (SEBC) as a practical way to recharge EVs on-road travel. In Figure 1, the SEBC system's concept is shown.

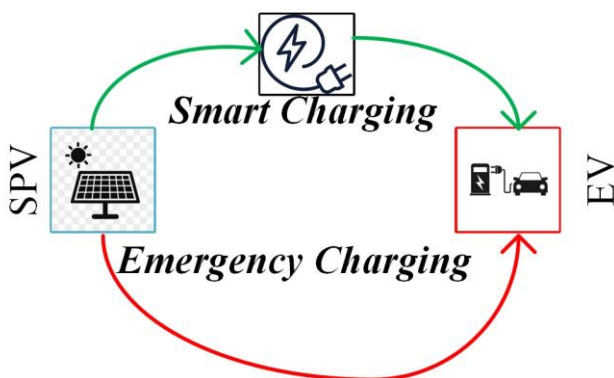


Fig. 1. Emergency Solar to Electric Vehicle Battery Charger.

By using this environmentally safe Electric Vehicle, each can contribute five to fifteen percent of the batteries energy to help

others in emergency situations. The output voltage and the current fed into the Electric vehicles are instantly adjusted in the suggested more innovative charging system. A Non-linear integral Back stepping controller (MF-NIBC) built on Deep Reinforcement Learnings (DRL) is used in the stability of electric vehicles. On the OPAL-RT platform, a real-time test is performed to see the applicability of the MF-NIBC controller.

This paper's section is organized as follows: The suggested SEBC's power structure, which consists of a unidirectional Dual Active Bridging (DAB) chopper, is discussed in Section 2. Section 3 presents the MF-NIBC design developed by DRL. The three scenarios real-time assertions are shown in Section 4 to verify the recommended controller. Finally, Section 5 brings the conclusion of the paper.

2. SUGGESTED SYSTEM LAYOUT

2.1. Power Layout of the Suggested SEBC

The suggested SEBC's power arrangement, which uses a unidirectional Dual Active Bridging (DAB) chopper, is shown in Figure 2. The dual active bridging design for DC-DC converter offers excellent efficiencies, great performances, an inbuilt soft-switching characteristic, more power density, and electrolytic separation (Feng et al., 2022). Additionally, the DAB has the ability to deliver unidirectional power flow, allowing for dynamic interaction with energy storage systems.

The two full bridge circuits are present in the DAB DC to DC converter and are coupled by a coupler inductor and an isolation transformer. The transformer leakage inductance supports the coupling inductor. The corresponding terminals of every bridge in the dual active bridging chopper produce square wave voltages. By properly correcting the coupling inductor, the power flow can be controlled, which flows from one DC source to another.

The voltage that is generated by the two bridges is shown as V_1 and V_2 , accordingly in Figure 2. In that i_L is the coupling inductor current, i_{out} is the output current, and i_{in} is the input current. The lag time between V_1 and V_2 to regulate power flow is equal to $\frac{dT_s}{2}$, in which d stands for duty cycle and T_s stands for switch period. The suggested SEBC chooses the best operation mode depending on the battery voltage level in the Electric Vehicles. In buck or boost modes, the DAB DC-DC converter must have functioned. The output current can be shown in the following when the converter is in buck mode.

$$I_{out} = \frac{nV_{in}T_s}{2L} (d - d^2) \quad (1)$$

Here n is the transformer's turn ratio. In Eq. (1), it is clear that a proper duty cycle can be used to regulate the SEBC's output current. Additionally, the converter's output curve could be written as follows in the boost mode and it is represented in Eq. (2).

$$I_{out} = \frac{nV_{in}T_s}{2L} (d^2 - d) \quad (2)$$

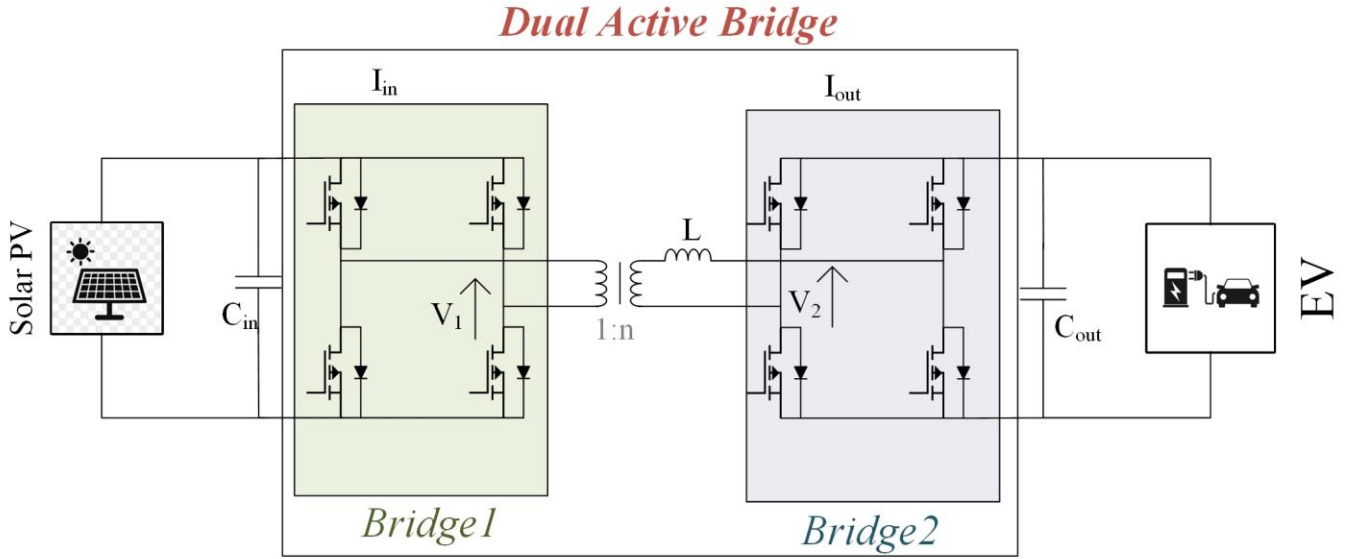


Fig. 2. Suggested SEBC's power Arrangement with DAB DC to DC converter.

Further information regarding the operational state of the DAB DC-DC converter occurs in (Naayagi et al., 2012). In this, dynamic stability analyses are carried out using the smaller signal model and the linear transfer functions. Figure 3 shows a simplified version of Figure 2, where R_s stands for the source's internal resistance. The following formula (Bai et al., 2010) (Vasuki et al., 2021) can be used to represent the smaller signal model of the DAB simple model which is represented in Eq. (3).

$$\begin{pmatrix} \frac{dv_1}{dt} \\ \frac{dv_2}{dt} \\ \frac{1}{R_s C_1} \\ 0 \end{pmatrix} = \begin{pmatrix} -\frac{1}{R_s C_1} & \frac{d^2-d}{2L f_s C_1} \\ -\frac{d^2+d}{2L f_s C_2} & -\frac{1}{R_s C_2} \end{pmatrix} \begin{pmatrix} V_1 \\ V_2 \end{pmatrix} + \begin{pmatrix} \frac{1}{R_s C_1} & \frac{2d-1}{2L f_s C_1} \\ -\frac{2d+1}{2L f_s C_2} & \frac{1}{R_s C_2} \end{pmatrix} \begin{pmatrix} V_s \\ \Delta * d \end{pmatrix} \quad (3)$$

Where Δ is the relatively % of the variation in the 2 square wave phase shifts. The following are some ways that the phase shifting duty cycle variations could affect the output voltage ripples content:

$$\frac{\Delta V_2}{V_2} = \frac{-2d+1}{4L f_s C_2} * \frac{V_1}{V_2} \quad (4)$$

According to Eq. (4), the DAB's stability may be ensured, and its quick, flexible response and absence of steady-state error can be controlled. In (Anitha et al., 2022) contains additional information regarding the stability of the DAB DC-DC converter. The technique for the controller design is provided in the following section.

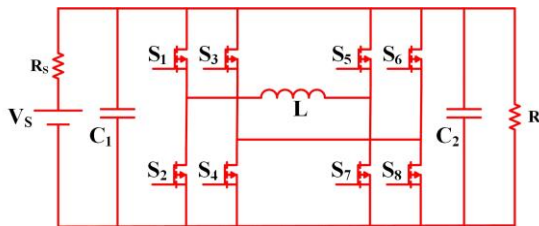


Fig. 3. Simplify DAB DC to DC Converter circuit.

2.2. Photovoltaic modelling

In terms of robustness with non-rotating equipment, high durability, good efficacy, and minimal maintenance among the many energy sources, solar PV is the best alternative option for producing power from PV without causing climate change. Cells in the PV system are connected in series to provide the required voltages. The photovoltaic plane of the final voltage is computed by combining the terminal voltage and the current. The corresponding model of a solar module is shown in Figure 4.

Eq. (5) and (6) are utilized to determine the output voltage and current requirements for solar panels.

$$I_{cp} = I_{sc} - I_o \left\{ \exp \left[\frac{Q}{TKA} (V_{cp} + I_{cp} R_{int}) - 1 \right] \right\} - \frac{V_{cp} + I_{sc} R_{int}}{R_{parallel}} \quad (5)$$

$$V_{cp} = \frac{TKA}{Q} \ln \left(\frac{I_{sc}}{I_{cp}} + 1 \right) \quad (6)$$

In this equation, Q stands for the charged particles, K for the diode component and Boltzmann equivalence, T for the temperatures (Kelvin), RSE for the series resistance, $R_{parallel}$ for the parallel resistance, I_{sc} for the current, and V_{cp} is cell potential. Lastly, Eq. (7) is used to calculate the solar panel's output power.

$$P_{solarPV} = N_{solarPV} * I_{solarPV} * V_{solarPV} \quad (7)$$

Where $P_{solarPV}$ stands for photovoltaic output, $I_{solarPV}$ for solar DC output current, $N_{solarPV}$ for the number of solar cells, and $V_{solarPV}$ for output voltages. Because of the limited capacity and consumption, peak power extraction from the system doesn't happen at all. To get the most power out of PV under various loads, maximum power point tracking is frequently permitted. There are various methods; the recommended method employs the incremental conductance technique.

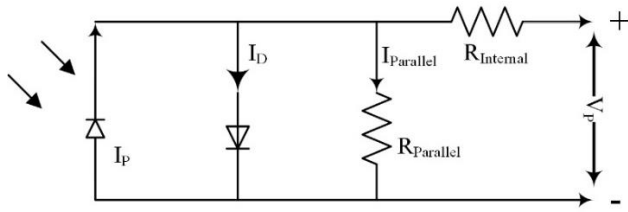


Fig. 4. Equivalent model of a solar module.

3. DEEP REINFORCEMENT LEARNING-BASED DESIGNING OF NOVEL ASSORT NON-LINEAR CONTROLLERS

The primary control goal is to react dynamically quickly and with zero steady-state error to govern the system of the researched SEBC. In this part, a deep reinforcement learning (DRL) algorithm-based Model Free Non-linear Integral Back stepping control (MF-NIBC) approach is recommended. Stabilization of MF-NIBC applied to the power converter system is examined using the basic Lyapunov theory approach.

The Lyapunov functions used for practical purposes have certain restrictions and correctness. One limitation is that these functions are only suitable for systems having particular features, such as steadiness, boundedness, and continuity. If the system does not exhibit these elements, then the Lyapunov function may be ineffective. Plus, the Lyapunov function must be selected cautiously so that the system is steady. If a Lyapunov function is chosen that is too intricate or too straightforward, it could be inadequate in depicting the dynamics of the system. Lastly, the Lyapunov function must be decided on so that it is easy to execute and can be calculated precisely. If the Lyapunov function is too intricate to carry out, or if it is not estimated accurately, then the outcomes may be inaccurate.

3.1. Model Free Integral Back Stepping Control (Mf-Nibc) Method Formation

The expression "model-free" is utilized to portray an assortment of procedures for tackling issues in an assortment of fields, including machine learning, reinforcement learning, artificial intelligence, and robotics. It is regularly utilized to allude to techniques that don't require a definite model of an arrangement or condition, however rather depend on trial and error or other learning-based techniques. Model-free strategies are regularly looked at with model-based strategies, which depend on express numerical models of the condition to make forecasts and choices.

Model-free control is a technique for tuning a control system without having to employ a mathematical model of the system. This form of control commonly utilizes a trial-and-error procedure, adjusting the controller parameters to get the wanted response. The objective of model-free control is to attain a desired performance with as little exertion as possible (Precup et al., 2022).

The SEBC system with the DAB DC to DC converter is shown in the next non-linear dynamics which is represented below in Eq. (8)

$$Y^n = F(y, \dot{y}, \ddot{y}, \dots, y^n) + gW \quad (8)$$

Wherein, $F(y, \dot{y}, \ddot{y}, \dots, y^n)$ is the take-out structure dynamics, W is the network input, and f is the unidentified scale element. Through describe $F_e(y, \dot{y}, \ddot{y}, \dots, y^n)$ and g' as uncertainty and Eq. (8) can be rewritten as follows using the unmodeled time vary forces at work of the suggested SEBC and the estimation of the unidentified scaling of constraint g is given below in Eq. (9),

$$Y^n = F(y, \dot{y}, \ddot{y}, \dots, y^n) + F_e(y, \dot{y}, \ddot{y}, \dots, y^n) + gW \quad (9)$$

Wherein η is the characterization of the command of the estimated models. So $F(y, \dot{y}, \ddot{y}, \dots, y^n)$ described in Eq. (10)

$$F_e(y, \dot{y}, \ddot{y}, \dots, y^n) = (\text{uncertainty and unmodeled dynamic system}) + (g - g')W, \quad (10)$$

To reduce the mistakes in certain state variables, an ultra-local model that is constantly remodeled could explain the input-output relationship of the proposed SEBC system (Glida et al., 2020) which is given by the Eq. (11) as follows,

$$x^n = F(y, \dot{y}, \ddot{y}, \dots, y^n) + gW \quad (11)$$

Wherein, $F(y, \dot{y}, \ddot{y}, \dots, y^n)$ is a continuous update function which explains the time vary changing aspects of battery charging systems and is defined in Eq. (12).

$$F(y, \dot{y}, \ddot{y}, \dots, y^n) + F_e(y, \dot{y}, \ddot{y}, \dots, y^n) = \text{continuous update function} \quad (12)$$

It is also possible to reduce the noise produced by the derivatives of y^n . As a result, the generic Model Free Control (MFC) input expression is given in Eq. (13).

$$W = \frac{-F(y, \dot{y}, \ddot{y}, \dots, y^n) + y_d^n - W_c}{g} \quad (13)$$

W_c is the feedback controllers' input, y_d^n is the nth derivative of the object path. Eq. (13) suggests that in order to alter the input control, based on the uncertainty of the system characteristics, with the co-ordinate of model-free and feedback controllers. Eq. (13) can be used in place of Eq. (11) to produce :

$$X^n = F(y, \dot{y}, \ddot{y}, \dots, y^n) + g \frac{-F(y, \dot{y}, \ddot{y}, \dots, y^n) + y_d^n - W_c}{g} = y_d^n - W_c \quad (14)$$

It is obviously seen the difference between each state variable desired and actual value in Eq. (14). So, the definition of the tracking error is given in Eq. (15) as:

$$e = y - y_d \quad (15)$$

Eq. (14) and (15) combined to give Eq. (16),

$$y^n - y_d^n + W_c = 0 = e^n + W_c = 0 \quad (16)$$

Here e^n is nth derivative of Eq. (15). Make sure that W_c must be designed in order to produce a linear differential equation that monotonically converges to the intended path.

The following Eq. (17) and (18) defines the variable of the SEBC system of the DAB DC to DC converter:

$$y_1 = v_{out} \quad (17)$$

$$y_2 = y_1 \quad (18)$$

The combination of the location errors of a given variable and the speed track errors associated with that particular specific state are the primary goals of MF-NIBC. So, the well-known Lyapunov function is used to guarantee the stabilization of the described Non-linear SEBC through errors of track convergent.

Lyapunov functions are advantageous for many practical applications as they present a mathematical way to analyze the steadiness of a system. The Lyapunov function can be used to gauge the steadiness of a system by studying how the value of the function adjusts over time. This can be employed to inspect the behavior of the system and deliver advantageous comprehension into how the system will respond to certain changes or inputs. In addition, Lyapunov functions can give a useful tool for constructing and optimizing control systems. By making use of Lyapunov functions, engineers can design systems that are more robust and proficient. Therefore, Lyapunov functions are a significant tool for practical applications.

In 1st step, positive definite Lyapunov function, $V(y_1 - y_1^d) = V(e_1)$ is generated within the desired state variable in following Eq. (19),

$$V(e_1) = \frac{1}{2} e_1^2 \quad (19)$$

By differentiating Eq. (19), we get Eq. (20) as,

$$V(e_1) = \frac{1}{2} (2e_1 \dot{e}_1) = e_1 (\dot{y}_2^d - \dot{y}_d) \quad (20)$$

The difference occurs between y_2 and y_2^d since y_2 is not the control Input of the system. So, to balance the dynamic error, the velocity tracking error is formulated as follows in Eq. (21) and Eq. (22),

$$e_2 = y_2 - y_2^d \quad (21)$$

$$e_2 = y_2 - \dot{y}_d + A e_1 \quad (22)$$

The system errors will settle to 0 if Lyapunov's function is accurately defined. To do this, Lyapunov's function is designed as semi-negative $V(e_1) \leq 0$. The Input y_2 described as Eq. (23),

$$y_2^d = \dot{y}_d - A e_1 \quad (23)$$

A steady state error can be produced by the specified SEBC system's uncertainty and the modelling error. This mistake might affect the controller's functionality. In order to eliminate this in the described controller, the integral terms given below are used in Eq. (24) and Eq. (25):

$$y_2 = \dot{y}_d - A e_1 - B \int e_1 \quad (24)$$

$$e_2 = y_2 - \dot{y}_d + A e_1 + B \int e_1 \quad (25)$$

The derivation of the location and velocity tracking error can be described as in Eq. (26) and (27),

$$e_1 = y_1 - y_d = e_2 + y^* - y_d = e_2 - A e_1 - B \int e_1 \quad (26)$$

$$e_2 = y_2 - \dot{y}_d + A e_1 - B e_1 = \ddot{y}_2 - \ddot{y}_d + A e_2 - A^2 e_1 - AB \int e_1 - B e_1 \quad (27)$$

The Lyapunov function $V(e_1, \int e_1)$ and $V'(e_1, e_2 \int e_1)$ is designed for the location and location speed tracking error and as mentioned below in Eq. (28), (29), (30) and (31)

$$V(e_1, \int e_1) = \frac{1}{2} [e_1^2 + B (\int e_1)^2] \quad (28)$$

$$V'(e_1, \int e_1) = e_1 \dot{e}_1 + B e_1 \int e_1 = e_1 (\dot{e}_2 - B e_1) \quad (29)$$

$$V'(e_1, e_2 \int e_1) = \frac{1}{2} [e_1^2 + e_2^2 + B (\int e_1)^2] \quad (30)$$

$$V'(e_1, e_2 \int e_1) = e_2 \dot{e}_2 + e_1 (\dot{e}_1 + B (\int e_1)) = e_1 (\dot{e}_2 - A e_1) + e_2 (\dot{y}_2 - \dot{y}_d - A^2 e_1 - B e_1 + A e_1 - AB \int e_1) \quad (31)$$

According to Lyapunov's theory, e_2 convergent to '0' by selecting semi-negative definite $V'(e_1, e_2)$ and Eq. (32) is given by,

$$e_1 \dot{e}_2 + e_2 (\dot{y}_2 - \dot{y}_d - A^2 e_1 - B e_1 + A e_1 - AB \int e_1) = -C e_2^2 \quad (32)$$

So, \dot{y}_2 could be defined as follows in Eq. (33),

$$\dot{y}_2 = F(y, \dot{y}, \ddot{y}) + \dot{y}_d + W_c = \dot{y}_d + (A^2 + B - 1)e_1 - (A + C)e_2 + AB \int e_1 \quad (33)$$

The system regulating law for the given SEBC with the dual active bridging chopper may thus be derived as , Eq. (23) by replacing Eq. (33) with Eq. (32) and is derived as Eq. (34),

$$W_c = (A^2 + B - 1)e_1 - (A + C)e_2 + AB \int e_1 - F(y, \dot{y}, \ddot{y}) \quad (34)$$

Figure 5 shows the NIB-MFC structure in accordance with the control law of W_c in Eq. (34).

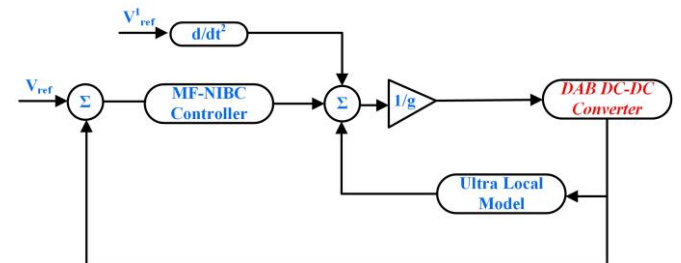


Fig. 5. NIB-MFC looping control system structure.

Since the controlling characteristics determine how effective the suggested MF-NIBC controller is, these variables are constructed using the deep deterministic policy gradient technique (DDPG). The computational complexity of Model Free Integral Back Stepping Control to design the controller is $O(n^3)$, where n is the number of states and control inputs.

3.2. Mechanism and Stability for DDPG

The Deep Deterministic Policies Gradients procedure offers the benefits of deterministic Policies Gradients (DPG) and Deep Q Networks (DQN). While the DQN-agent implements the Epsilon-Greedy policies and does distinct operations, the deep neural network (DNN) approximates the Q-function in Q-learning. By configuring the DNN, wherein the weights coefficient of the system is developed by the efficiency of the policy's gradients. The four deep neural networks, comprising the primary actor and critics networks and the objective network, make up the DDPG algorithms.

The steadiness of DDPG is reliant on multiple elements, including the selection of the neural network pattern, the learning rate, the exploration approach, and the reward system. The pick of neural network blueprint is pertinent since it affects the intricacy of the policy being learned. A complicated network with a lot of layers and nodes can often cause unsteadiness due to the augmented number of parameters that can be adjusted. Also, the number of neurons in each layer should be decided on carefully because too many neurons can cause overfitting. The learning rate is indispensable for the steadiness of DDPG. If the learning rate is too high, the algorithm might become unstable and not converge. On the other hand, if the learning rate is too low, the algorithm may take too long to converge. It is thus important to find an optimal learning rate that guarantees steadiness while still allowing the algorithm to converge. The exploration policy is also a critical factor in the steadiness of DDPG. The policy should be chosen in a way that motivates exploration without causing unsteadiness. For instance, a policy that randomly explores without any control can lead to unsteadiness due to the randomness of the exploration.

To analyze the stability of the DDPG algorithm, we can examine its underlying equations. These equations can be broken down into two main parts: the actor-critic update and the target network update. The actor-critic update works to optimize the expected total reward by implementing the Bellman equation to compute the Q-value of the current state-action pair. The gradients of the Q-value are then used to modify the actor and critic networks. To balance the learning process, the target network update is utilized to offer a slowly changing objective for the Q-value. This is accomplished by allocating the target network parameters to a moving average of the actor-critic network parameters.

In the DDPG approach, the critics networks are trained to use a deep neural network instead of the Q table, while the actor-

network is trained to provide determinists policies (Qiu et al., 2019), (Gheisarnejad et al., 2021).

The computational intricacy of Deep Deterministic Policies Gradients (DDPG) to construct the controller is $O(N)$, where N stands for the amount of parameters in the neural network. DDPG is an off-policy, actor-critic reinforcement learning algorithm not requiring a model and taking advantage of a deep neural network as the controller. The complexity of DDPG is determined by the magnitude of the neural network, which is based on the quantity of parameters.

In policy gradients, where states are mapped to actions based on probabilities, the progress of the agent is dependent on the policy p . The q table described in the Bellman's eqn (Wei et al., 2022) by taking into account the action W_t and state S_t under a deterministic policy of activities $q^\mu(S_t, W_t)$ is given by Eq. (35):

$$q^\mu(S_t, W_t) = E_{r_t, s_{t+1} \sim \Phi[r(S_t, W_t)]} + g[q_{(S_{t+1}, \mu(S_{t+1}))}^\mu] \quad (35)$$

Here r stands for the reward function, g for the discount factors, and Φ for the distributions of expectations. Deep neural networks q are predicted to be able to approximate the Bellman equation for a random stochastic policy Φ . The critic network's update loss is calculated using Eq. (36):

$$L(\theta^q) = E_{s \sim p} \Phi, W \sim \mu \sim \Phi [q^\mu(S_{t+1}, \mu(S_{t+1})) - y_t]^2 \quad (36)$$

p^Φ stands for the state distributions under the F policy, θ^q is the deep q -network weight variable, and x_t is well-defined as in Eq. (37):

$$x_t = r(S_t, W_t) + \gamma Q(S_{t+1}, \mu(S_{t+1})) \theta^q \quad (37)$$

The respective gradient updates the response network's policy with the critic network and is given by Eq. (38),

$$\nabla_{\theta^\mu} J^{\theta^\mu} \approx E_{s \sim \rho^\mu} [\nabla_w q(s, w | \theta^q) |_{s=s_t, w=\mu(s_t)} \nabla_{\theta^\mu} \mu(s | \theta^\mu) |_{s=s_t}] \quad (38)$$

- 1: Randomly initialize critic Q and actor μ networks with weights θ^Q and θ^μ
- 2: Initialize target networks Q' and μ' with weights $\theta^{Q'} \leftarrow \theta^Q, \theta^{\mu'} \leftarrow \theta^\mu$
- 3: Set up empty replay buffer R
- 4: for episode = 1 to M do
- 5: Begin with an Ornstein-Uhlenbeck (OU) noise \mathcal{N} for exploration
- 6: Receive initial observation state
- 7: for $t = 1$ to T do
- 8: Apply action $a_t = \mu(s_t | \theta^\mu) + \mathcal{N}$ to environment
- 9: Observe next state s_{t+1} and reward r_t
- 10: Store following transitions (s_t, a_t, r_t, s_{t+1}) into replay buffer R
- 11: Sample random minibatch of K transitions from R
- 12: Set $y_i = r_i + \gamma Q'(s_{i+1}, \mu'(s_{i+1}) | \theta^{\mu'}) | \theta^{Q'}$
- 13: Update critic by the loss: $L = \frac{1}{N} \sum_{i=1}^N (y_i - Q(s_i, a_i | \theta^Q))^2$
- 14: Update the actor policy using the sampled policy gradient:
$$\nabla_{\theta^\mu} J^{\theta^\mu} \approx \frac{1}{N} \sum_i \nabla_a Q(s, a | \theta^Q) |_{a=\mu^\theta(s)} \nabla_{\theta^\mu} \mu(s | \theta^\mu)$$
- 15: Update the target networks:
$$\theta^{Q'} \leftarrow \tau \theta^Q + (1 - \tau) \theta^{Q'}, \theta^{\mu'} \leftarrow \tau \theta^\mu + (1 - \tau) \theta^{\mu'}$$
- 16: end for
- 17: end for

Fig. 6. The DDPG algorithm's process.

Here θ^μ stands for the actor DNN's weight variable. Figure 6 illustrates the DDPG algorithm's procedure code(Farag, 2020).

The DDPG includes a replay buffer to eliminate sample relationships and improve training stability by isolating the target DNNs (q', μ'). For exploratory reasons, additional noise N is also added to the actions so that $w_t = \mu(S_t) + N$. Additionally, update the critics and actor target network is given in Eq. (39) and (40),

$$\theta^{q'} \leftarrow \tau\theta^Q + (1 - \tau)\theta \tag{39}$$

$$\mu^{q'} \leftarrow \tau\theta^\mu + (1 - \tau)\mu \tag{40}$$

3.3. Utilizing the MF-KEY NIBC'S Constants

The MF-NIBC controller's structure contains a few variables that must be properly changed in order to control the outcome of the dual active bridging chopper. Elements of A, B, as well as C, are the essential variables in MF-NIBC laws regulation Eq. (31) that the DDPG algorithm will customize it. Figure 7 shows the general layout of the suggested DDPG-based MF-NIBC controller.

In this methodology, the system states are represented by the terms of the output voltages V_o and the trailing errors $e(t) = v_o(t) - v_{ref}(t)$, the lag of the voltages errors ($e_d(t)$), and the derivation value of v_o and $e(t)$. $s_t = (v_o(t), e(t), v_{o-d}(t), e_d(t), v_o(t)/dt, de(t)/dt)$. By maximizing the reward function, the DDPG-deep agent's neural network is trained to reduce output power fluctuation in the power electronics tests. The definition of the reward signal is defined as following Eq. (41):

$$r_t = \begin{cases} \frac{\sigma_2}{|v_o(t) - v_{ref}(t)|}, & \text{if } (v_o(t) - v_{ref}(t)) < \epsilon \\ -\sigma_1 |v_o(t) - v_{ref}(t)|, & \text{else} \end{cases} \tag{41}$$

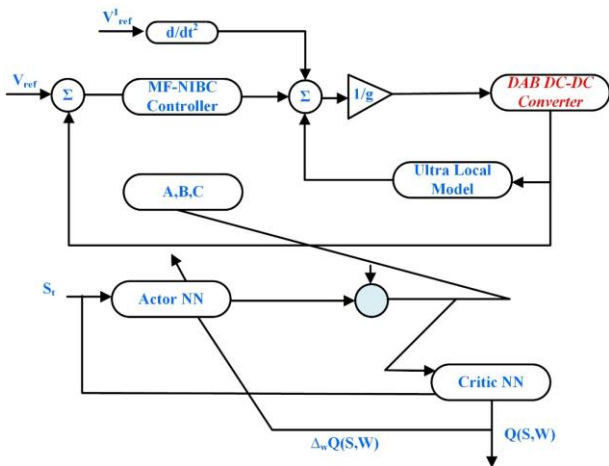


Fig. 7. DDPG Algorithm based MF-NIBC controller.

Here ϵ is the specified Output voltage deviation from the nominal value σ_1 and σ_2 are the reward penalties. The DDPG agent adjusts the control settings to maximize a reward signal, which stabilizes the Output voltage by utilizing the neural network's capabilities. Figure 8 shows the DDPG algorithm's deep neural network architecture.

The DDPG agent adjusts the control variables to maximize a reward signal while stabilizing the Output voltage. Figure 8

shows the DDPG algorithm's deep neural network architecture.

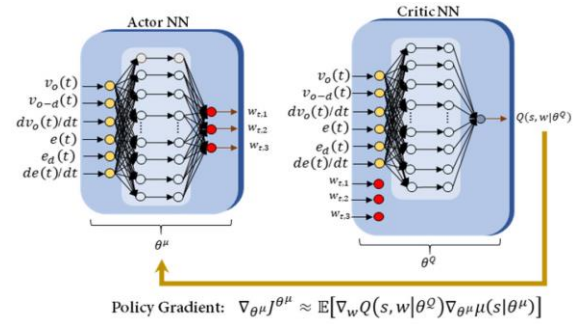


Fig. 8. The actor-critic DDPG algorithm structure.

4. PERFORMANCE ASSESSMENT

The real-time findings are described in this part to verify the efficiency of the suggested controllers and the functionality of the smart chargers. Figure 9 depicts the setup test based on the OPAL-RT. Table 1 lists the electrical specifications for the proposed Electric vehicle smart charger, and Table 2 lists the controller specifications. On the basis of the electrical specifications of the EV's battery, a number of criteria can be taken for granted to examine the applicability of the suggested Emergency Solar to Electric vehicle battery charger (SEBC). Based on the battery's voltage, three situations can be examined for this reason.



Fig. 9. SEBC's Real Time setting is based on OPAL-RT.

Table 1. Variables of the SEBC.

Variables	Values	Variables	Values
V_{in}	400 v	C_{out}	200 μ F
V_{out}	300 – 500 v	L	40 μ H
I_{rated}	20 A	N	2.5
P_{rated}	8000 W	C_{in}	20 μ F

Table 2. Variables of the Controllers.

Variables	Values
K_p	0.003
K_i	25
Predicting Horizon (N)	6
Weigh Factor (λ)	0.5

Case 1: In the first case, the assumption is both EVs' batteries are identical. As a result, the DAB DC-DC converter's Input and Output voltages are 400 Volts and 20 Ampere, respectively. In this case, the correct value and charge rate are established by controlling the DAB DC-DC converter's Output current. As seen in Figure 10a, the converter's maximum current in emergency mode is set to be 25 Ampere at 400 Volts. The maximum amount of transmitted energy in this circumstance is 15 percent of the battery's capacity. Additionally, there is a restriction of current of 15 Ampere on the current transmission of one Electric vehicle to another Electric Vehicle.

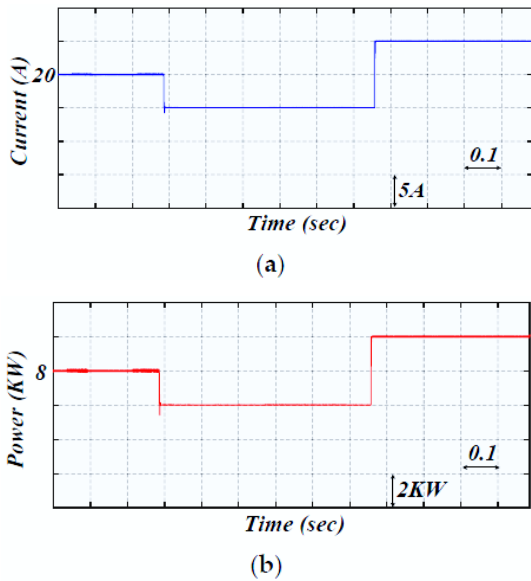


Fig. 10. Performance for the emergency charging mode in the projected SEBC in a real-time basis: (a) Output Current (b) Output Power.

The suggested SEBC's Output current and power step changes are depicted in Figures 10a and 10b, respectively. Figure 11 displays the suggested charger's Output voltage. A relationship between the MPC controller and the traditional PI controller is done in order to show how well our suggested charger performs with the innovative MF-NIBC controller. Figure 11 shows that suggested controllers have a higher transient response and ensure the stabilization of the DAB DC to DC converter's Output voltage. Furthermore, the simultaneous realization of Output current control is possible.

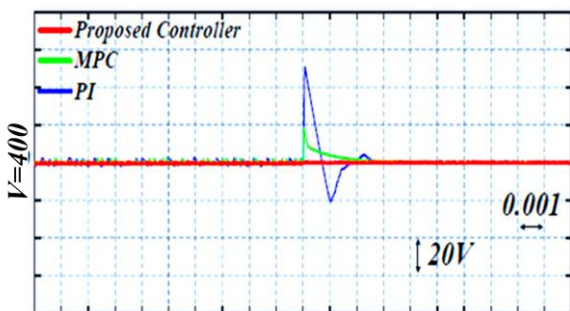


Fig. 11. While step change in the Output power in the 1st case, the correlation of voltage transitory response of the suggested MF-NIBC controllers, MPC, and the traditional PI controllers.

Case 2: The Electric batteries in the 2nd case are seen as being different. It indicates that the 2nd Electric Vehicle, which receives the energy, is supposed to have a voltage of 300 Volts, while the first EV, which injects power into the other, has a voltage of 400 Volts. The highest and lowest values of the current that can be injected in this case are 25 A and 15 A, accordingly. The spontaneous results of the Output voltages of the suggested charging system are depicted in Figure 12 to demonstrate the advantages of the MF-NIBC controller over other controllers. The MF-NIBC controller has the quickest transitory responses compared to other controllers, which means the proposed method can provide voltage stabilization and offer correct controlling of the Output voltages and current simultaneously. This conclusion can be drawn from Figure 12.

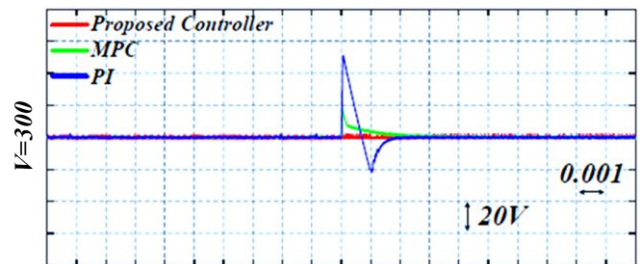


Fig. 12. Performance of suggested MF-NIBC controller, MPC, and the traditional PI controller's voltage transitory responses during a step change in Output power in 2nd case.

Case 3: In the final case, it is considered that the second Electric vehicle's nominal voltage is 500 Volts while the Electric vehicle acting as a source has a voltage of 400 Volts. As earlier mentioned, because the SEBC operates in crisis mode, it is permitted to transmit up to 15% of the battery's capacity. As a result, the injected current is restricted within top and bottom preset values, as shown in Figure 10a. The transient results of the suggested MF-NIBC controllers, MPC controllers, and PI controllers are expressed in Figure 13. Figure 13 proposed smooth charging system has high reliability with the least overshoots when compared with conventional controllers with the support of proposed MF-NIBC controllers.

Employing same design goals and complexity, the following controller's objectives are designed: Employ a consistent design procedure with a clear definition of the problem, the anticipated result, the intended audience, and the assessment criteria. Create a design specification that lists the features and functions of the controller based on customer feedback and market research. Utilize a modular system to the design process, dividing the controller into smaller segments that can be designed and tested separately. Adopt a top-down design approach, starting with the general system architecture and later focusing on the details. Implement a standard set of components and parts for all controllers to guarantee that the complexity of each controller is consistent. Utilize existing design patterns and industry standards to guarantee the controllers are designed with efficiency and effectiveness. Put into effect a rigorous testing process to make sure that all controllers meet the design objectives and possess a consistent level of complexity.

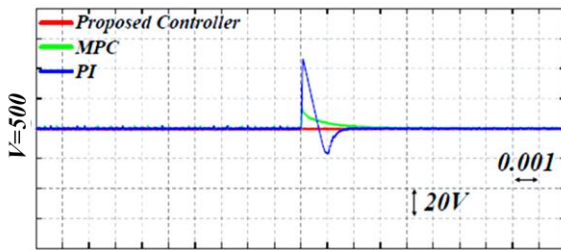


Fig. 13. The comparison of the proposed MF-NIBC controller, MPC, and the traditional PI controller voltage transient responses during a step change in Output power in the 3rd case.

5. CONCLUSION

This study presents the development of an Emergency solar-to-Electric vehicle Portable Battery Charger (SEBC) for charging Electric vehicles in emergency mode while driving. The suggested smart charging system can distribute up to 15% of the energy that has been stored, which is taken into account capacity, state of charging (SOC), and other significant methodological specifications of the Electric Vehicle batteries. The suggested SEBC can continuously control the Output voltages and the injecting current to the Electric vehicle by utilizing a Dual Active Bridge (DAB) chopper. A model Free non-linear integrals backstepping controller (MF-NIBC) was done to control the Output voltages of the suggested SEBC to achieve smart charging processes. Additionally, a deep deterministic policy gradient (DDPG) was used in conjunction with the actor and critic network to modify the MF-NIBC controller. The functionality and viability of the suggested SEBC were validated using real-time data based on the OPAL-RT configuration. Long-term analysis of the transferred energy and conversion efficiency is required for future work. Additionally, the temperature that both batteries encounter should be examined while taking into account how the transfer affects the progression of temperature.

REFERENCES

- Abouddrar, I., Hani, S. El, El Harouri, K., Martins, J., & Goncalves, R. J. (2020). Reactive Power Compensation by ADRC in Vehicle to Grid Application during Grid Fault Conditions. *2020 International Conference on Electrical and Information Technologies, ICEIT 2020*. <https://doi.org/10.1109/ICEIT48248.2020.9113222>
- Ahmed, I., Ahmad, I., Ahmed, S., & Adil, H. M. M. (2021). Robust nonlinear control of battery electric vehicle charger in grid to vehicle applications. *Journal of Energy Storage*, *42*, 103039. <https://doi.org/10.1016/J.EST.2021.103039>
- Anitha, P., Kumar, K. K., Ravindran, M., & Saravanaselvan, A. (2022). Evolutionary Algorithm Based Z-Source DC-DC Boost Converter for Charging EV Battery. *Intelligent Automation & Soft Computing*, *34*(2), 1377–1397. <https://doi.org/10.32604/IASC.2022.025396>
- Asna, M., Shareef, H., Achikkulath, P., Mokhlis, H., Errouissi, R., & Wahyudie, A. (2021). Analysis of an Optimal Planning Model for Electric Vehicle Fast-Charging Stations in Al Ain City, United Arab Emirates. *IEEE Access*, *9*, 73678–73694. <https://doi.org/10.1109/ACCESS.2021.3081020>
- Bai, H., Nie, Z., & Mi, C. C. (2010). Experimental comparison of traditional phase-shift, dual-phase-shift, and model-based control of isolated bidirectional dc-dc converters. *IEEE Transactions on Power Electronics*, *25*(6), 1444–1449. <https://doi.org/10.1109/TPEL.2009.2039648>
- Chang, M., Bae, S., Cha, G., & Yoo, J. (2021). Aggregated Electric Vehicle Fast-Charging Power Demand Analysis and Forecast Based on LSTM Neural Network. *Sustainability 2021, Vol. 13, Page 13783, 13*(24), 13783. <https://doi.org/10.3390/SU132413783>
- Dumitrache, I., Caramihai, S. I., Popescu, D. C., Moisescu, M. A., & Sacala, I. S. (2021). Neuro-inspired Framework for Cognitive Manufacturing Control. *INTERNATIONAL JOURNAL OF COMPUTERS COMMUNICATIONS & CONTROL*, *16*(6). <https://doi.org/10.15837/IJCCC.2021.6.4519>
- Farag, W. (2020). Multi-Agent Reinforcement Learning using the Deep Distributed Distributional Deterministic Policy Gradients Algorithm. *2020 International Conference on Innovation and Intelligence for Informatics, Computing and Technologies, 3ICT 2020*. <https://doi.org/10.1109/3ICT51146.2020.9311945>
- Feng, H., Teng, F., Montes, O. A., Awal, M. A., Bipu, M. R. H., Husain, I., & Lukic, S. (2022). Passive Capacitor Voltage Balancing of SiC-Based Three-Level Dual-Active-Bridge Converter Using Hybrid NPC-Flying Capacitor Structure. *IEEE Transactions on Power Electronics*, *37*(4), 4183–4194. <https://doi.org/10.1109/TPEL.2021.3119210>
- Fuinhas, J. A., Koengkan, M., Leitão, N. C., Nwani, C., Uzuner, G., Dehdar, F., Relva, S., & Peyerl, D. (2021). Effect of Battery Electric Vehicles on Greenhouse Gas Emissions in 29 European Union Countries. *Sustainability 2021, Vol. 13, Page 13611, 13*(24), 13611. <https://doi.org/10.3390/SU132413611>
- Gheisarnejad, M., Farsizadeh, H., Tavana, M. R., & Khooban, M. H. (2021). A Novel Deep Learning Controller for DC-DC Buck-Boost Converters in Wireless Power Transfer Feeding CPLs. *IEEE Transactions on Industrial Electronics*, *68*(7), 6379–6384. <https://doi.org/10.1109/TIE.2020.2994866>
- Gheisarnejad, M., & Khooban, M. H. (2019). Supervised control strategy in trajectory tracking for a wheeled mobile robot. *IET Collaborative Intelligent Manufacturing*, *1*(1), 3–9. <https://doi.org/10.1049/IET-CIM.2018.0007>
- Glida, H. E., Abdou, L., Chelihi, A., Sentouh, C., & Hasseni, S. E. I. (2020). Optimal model-free backstepping control for a quadrotor helicopter. *Nonlinear Dynamics 2020 100:4*, *100*(4), 3449–3468. <https://doi.org/10.1007/S11071-020-05671-X>
- Gryparis, E., Papadopoulos, P., Leligou, H. C., & Psomopoulos, C. S. (2020). Electricity demand and carbon emission in power generation under high penetration of electric vehicles. A European Union perspective. *Energy Reports*, *6*, 475–486. <https://doi.org/10.1016/J.EGYR.2020.09.025>
- Iyer, V. M., Gulur, S., Gohil, G., & Bhattacharya, S. (2018). Extreme fast charging station architecture for electric vehicles with partial power processing. *Conference*

- Proceedings - IEEE Applied Power Electronics Conference and Exposition - APEC, 2018-March*, 659–665. <https://doi.org/10.1109/APEC.2018.8341082>
- Krishna, G. (2021). Understanding and identifying barriers to electric vehicle adoption through thematic analysis. *Transportation Research Interdisciplinary Perspectives*, 10, 100364. <https://doi.org/10.1016/J.TRIP.2021.100364>
- Li, Y., Li, L., Peng, C., & Zou, J. (2019). An MPC based optimized control approach for EV-based voltage regulation in distribution grid. *Electric Power Systems Research*, 172, 152–160. <https://doi.org/10.1016/J.EPSR.2019.03.003>
- Mallik, A., Lu, J., & Khaligh, A. (2018). Sliding Mode Control of Single-Phase Interleaved Totem-Pole PFC for Electric Vehicle Onboard Chargers. *IEEE Transactions on Vehicular Technology*, 67(9), 8100–8109. <https://doi.org/10.1109/TVT.2018.2848238>
- Naayagi, R. T., Forsyth, A. J., & Shuttleworth, R. (2012). High-power bidirectional DC-DC converter for aerospace applications. *IEEE Transactions on Power Electronics*, 27(11), 4366–4379. <https://doi.org/10.1109/TPEL.2012.2184771>
- Precup, R.-E., Roman, R.-C., & Safaei, A. (2022). *Data-driven model-free controllers*. <https://www.routledge.com/Data-Driven-Model-Free-Controllers/Precup-Roman-Safaei/p/book/9780367697303#>
- Qiu, C., Hu, Y., Chen, Y., & Zeng, B. (2019). Deep Deterministic Policy Gradient (DDPG)-Based Energy Harvesting Wireless Communications. *IEEE Internet of Things Journal*, 6(5), 8577–8588. <https://doi.org/10.1109/JIOT.2019.2921159>
- Sheng, K., Dibaj, M., & Akrami, M. (2021). Analysing the Cost-Effectiveness of Charging Stations for Electric Vehicles in the U.K.'s Rural Areas. *World Electric Vehicle Journal 2021, Vol. 12, Page 232, 12(4)*, 232. <https://doi.org/10.3390/WEVJ12040232>
- Song, J., Fu, C., Zhang, G., Duan, B., & Zhang, C. (2021). Backstepping Control of High-Frequency Link Matrix Rectifier for Battery Chargers. *IEEE Transactions on Power Electronics*, 36(9), 10801–10814. <https://doi.org/10.1109/TPEL.2021.3063418>
- Tu, H., Feng, H., Srdic, S., & Lukic, S. (2019). Extreme Fast Charging of Electric Vehicles: A Technology Overview. *IEEE Transactions on Transportation Electrification*, 5(4), 861–878. <https://doi.org/10.1109/TTE.2019.2958709>
- Ucgun, H., Okten, I., Yuzgec, U., & Kesler, M. (2022). Test Platform and Graphical User Interface Design for Vertical Take-Off and Landing Drones Test Platform and Graphical User Interface Design for Vertical Take-Off and Landing. In *ROMANIAN JOURNAL OF INFORMATION SCIENCE AND TECHNOLOGY (ROMJIST) (Vol. 25)*.
- Vasuki, G., Vinothini, M., Rushmithaa, S. B., Kumar, K. K., Kamaraja, A. S., & Iruthayarajan, M. W. (2021). 13-level Inverter Configuration with a Reduced Auxiliary Circuit for Renewable Energy Applications. *Proceedings of the 5th International Conference on Electronics, Communication and Aerospace Technology, ICECA 2021*, 101–105. <https://doi.org/10.1109/ICECA52323.2021.9675929>
- Wei, Z., Quan, Z., Wu, J., Li, Y., Pou, J., & Zhong, H. (2022). Deep Deterministic Policy Gradient-DRL Enabled Multiphysics-Constrained Fast Charging of Lithium-Ion Battery. *IEEE Transactions on Industrial Electronics*, 69(3), 2588–2598. <https://doi.org/10.1109/TIE.2021.3070514>
- Wu, X., Liu, Z., Du, J., & Yu, B. (2021). Research on Zero Voltage Switching Non-inductive Current Circulation Control of Bidirectional DC/DC Converter for Hybrid Energy Source System of Electric Vehicle. *Journal of Electrical Engineering & Technology 2020 16:2, 16(2)*, 873–887. <https://doi.org/10.1007/S42835-020-00610-7>
- Younes, Y. Al, Drak, A., Noura, H., Rabhi, A., & Hajjaji, A. El. (2016). Robust Model-Free Control Applied to a Quadrotor UAV. *Journal of Intelligent & Robotic Systems 2016 84:1, 84(1)*, 37–52. <https://doi.org/10.1007/S10846-016-0351-2>
- Zamfirache, I. A., Precup, R. E., Roman, R. C., & Petriu, E. M. (2022). Policy Iteration Reinforcement Learning-based control using a Grey Wolf Optimizer algorithm. *Information Sciences*, 585, 162–175. <https://doi.org/10.1016/J.INS.2021.11.051>
- Zeitouni, M. J., Parvaresh, A., Abrazeh, S., Mohseni, S. R., Gheisarnejad, M., & Khooban, M. H. (2020). Digital Twins-Assisted Design of Next-Generation Advanced Controllers for Power Systems and Electronics: Wind Turbine as a Case Study. *Inventions 2020, Vol. 5, Page 19, 5(2)*, 19. <https://doi.org/10.3390/INVENTIONS5020019>